Microwave Dielectric Characterization of Microplatelets and Emulsions

Ali Abduljabar [a], Hayder Hamzah [b], and Adrian Porch [c]

a Engineering College, University of Basrah, Basrah IQ-61002, Iraq (e-mail: aliaiq76@gmail.com).
b Engineering College, University of Al-Qadisiyah, Al-Qadisiyah 58001, Iraq (e-mail: hayder.hamzah@qu.edu.iq), corresponding author.
c Centre for High Frequency Engineering, Cardiff University, Cardiff CF10 3AT, U.K. (e-mail: porcha@cardiff.ac.uk).

Abstract

A compact microwave sensor incorporating a dual central gap, split ring resonators (DCGRR) is proposed in this paper for microplatelet detection, characterization and dielectric measurements within a microfluidic channel passing through the capacitive regions which act as the sensing zones. The sensor was designed, optimized and fabricated using COMSOL Multiphysics. The dual resonators operate at resonant frequencies of 2.36 and 2.68 GHz, respectively. Measurements of the microplatelets were carried out within a water solvent, with good agreement between the simulated and measured results. Furthermore, the sensor was tested with emulsions at different concentrations to confirm the sensor's ability to detect small changes in emulsion concentration at the two resonant frequencies. The experimental results demonstrate the high sensitivity of resonant frequency to emulsion water content.

Keywords

Microwave sensing, microplatelet detection, split ring resonator, resonant sensor.

1. Introduction

Detection and identification of micro-particles inside high purity materials is an important issue as the existence of these unwanted impurities, such as metallic or non-metallic particles, may degrade the quality of the product. Microwave technology can provide an attractive detection system due to its ability to penetrate deeply inside materials [1]. Hence the use of microwave technology is of great interest for industrial, chemical, pharmaceutical, and healthcare applications, and in the determination of material characteristics and structural composition [2-6]; examples include dielectric measurements of liquids [7, 8] and solid dielectric materials [9, 10], biosensors and applicators in medical and biological applications [11-15].

Furthermore, intensive research has been conducted in the use of microwave techniques to develop efficient, consistent, accurate and non-invasive bio-sensors. Recently, the use of microwave techniques in the detection of human cells via their dielectric properties has produced important results [12, 16]. Dielectric spectroscopy using microwaves has been demonstrated as a promising technology to investigate membrane permeabilization and its effects on chemotherapy-induced cells [17]. In addition, dielectric properties analysis methods which operate at microwave frequencies can provide an abundant range of bio-information, dependent on the molecular content of the tested medium, i.e., dielectric polarization of molecules as a response to the electric field and the interactions between molecules, in particular [18, 19].

Microwave biosensors have been used to investigate the dielectric property of single cells, which pass along a microfluidic channel through a capacitive sensing gap [18, 20-22]. For the examination of living cells, microwaves have an advantage in their electromagnetic fields penetrate (and so detect) deeply inside the intracellular content, thus providing powerful information about the tested medium and hence the physiological condition of the cells [18, 23].

In [24], a miniaturized microwave-based biosensor was developed to identify living and dead cells through their dielectric properties; in [25], a system was designed to detect biomaterials in various suspension fluids using a transmission line microwave resonator integrated into an interferometer. A microwave hairpin resonator integrated with microfluidic channel was used in [26] for the detection of biological cells. The microwave-based biosensor was a microfluidic device fabricated from polydimethylsiloxane (PDMS) and negative photoresist (SU-8) to measure and characterize biological cells in a liquid medium. The detection of biological cells was based on measuring the scattering parameters (S_{11} and S_{21}) at a resonant frequency of 2.17 GHz. In spite of the sensitivity limitation, they demonstrated the potential of hairpin resonator sensors for the analysis of biological cells.

Moreover in [27] the split ring microwave sensor has been used to measure Escherichia coli bacteria concentration in real time.

Nevertheless, most of these works are devoted to dielectric evaluations of cell groups rather than to single cell properties. More and more data in other clinically and pre-clinically performed research indicates that a single cell heterogeneity is a major feature of most cancers when monitoring pathogenic signals. In this context, real-time process quality control is a major concern and microwave technology will provide higher adaptability and versatility compared to conventional chemical processes, at a relatively low cost. A variation of the complex dielectric permittivity is generated depending on the form and quantity of a chemical component in the liquid under test.

Another important application of the microwave liquid sensors is the monitoring the concentrations of emulsions. An active microstrip sensor has been proposed in [28, 29] to measure the concentration of asphaltene where active loop feedback is added to increase the quality factor.

In this work, we present a new application for a microwave central gap ring resonator (CGRR) to detect, measure the dielectric properties, and characterize the shape of micro-platelets. This was achieved by modifying the design in [30] and adding a second resonator and packaging them in a single compact sensor, providing two dielectric sensing zones, as will be demonstrated in this paper. The electric field orientations in the two gaps are perpendicular to each other, thus providing complementary dielectric and geometrical information about the micro-platelets. Our proposed sensor was tested with emulsions at different concentrations. The detection is based on the change in each sensor's resonant frequencies, which decrease with higher emulsion dielectric constant due to the higher water content.

2. Theory of Microwave Sensing

A. Liquid Sensing

Dielectric sensing and measurement using resonant microwave sensors is based on cavity perturbation theory. When placing a dielectric sample in a high electric field, a reduction in both resonant frequency and quality factor Q will occur due to the sample material's polarization and dielectric loss, respectively. Due to this interaction between the microwave electric field and sample under test SUT, the dielectric properties can be measured and evaluated, where this interaction depends on the complex relative permittivity $\varepsilon_r = \varepsilon_1 - j\varepsilon_2$ of the sample material, which for polar liquids (such as water) is well-described by the Debye model [31].

When a microwave electric field E_0 is applied perpendicular to the axis of a capillary containing a polar liquid, the microwaves will penetrate the liquid, giving rise to a uniform internal electric field and a net dipole moment of

$$p \approx \left[\frac{(\varepsilon_{rc}-1)(\varepsilon_{rc}+\varepsilon_{rl}) + \left(\frac{r_1}{r_2}\right)^2 (\varepsilon_{rc}+1)(\varepsilon_{rc}-\varepsilon_{rl})}{(\varepsilon_{rc}+1)(\varepsilon_{rc}+\varepsilon_{rl}) + \left(\frac{r_1}{r_2}\right)^2 (\varepsilon_{rc}-1)(\varepsilon_{rc}-\varepsilon_{rl})}\right] \varepsilon_0 \, E_0 \, V_s \tag{1}$$

In (1), ε_{rc} and ε_{rl} are the relative permittivity of the capillary and liquid, respectively, r_2 and r_1 are outer and inner radii of the capillary, respectively, V_s is the liquid volume within the electric field and ε_0 is the permittivity of free space.

Our sensor design uses central gap ring resonators, as shown in Fig. 1; the resonators are actually stacked on the same axis but are here shown side-by-side for clarity. The idea of this new design is to characterize the sample (micro-plates or emulsion) from two perpendicular directions instead of one direction as in previous works such as [27] where more information can be obtained especially when the sample material is inhomogeneous. The resonant frequency, f_r, of such a lumped element resonator is:

$$f_r = \frac{1}{2\pi\sqrt{LC}} \tag{2}$$

where L and C are the inductance and capacitance, respectively. The capacitance C is associated with the electric field in the gap region, which is where the perturbation occurs. Changes in both resonant frequency Δf and loss $\Delta(1/Q)$ will occur according to simple cavity perturbation theory due to liquid sample's induced electric dipole moment p. These changes can be expressed in terms of the frequencies f_1 and f_0, and quality factors Q_1 and Q_0 of the resonator with and without liquid, respectively

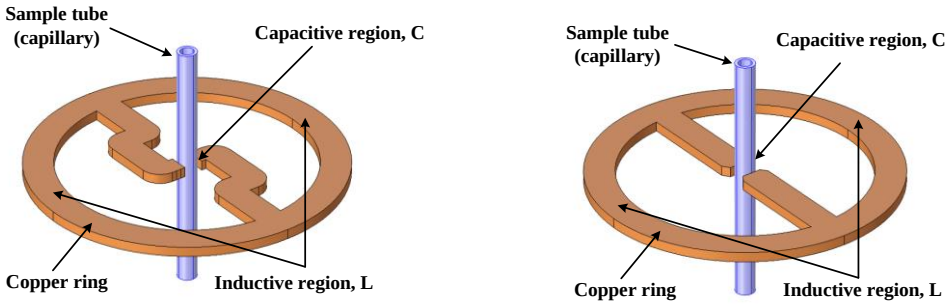

(a) (b)

Fig. 1. Central gap ring resonators which will be utilized in our sensor design.

$$\Delta f = f_1 - f_0 = -\frac{f_0}{4}\,\mathrm{Re}\left(\frac{pE^*_{app}}{U_{tot}}\right) \tag{3}$$

$$\Delta\left(\frac{1}{Q}\right) = \frac{1}{Q_1} - \frac{1}{Q_0} = -\frac{1}{2}\,\mathrm{Im}\left(\frac{pE^*_{app}}{U_{tot}}\right) \tag{4}$$

where U_{tot} is the resonator's averaged stored energy.

B. Microspheres/Microplatelets in a Solvent Medium

A sample's polarizability α is its dipole moment p induced per applied electrical field E_{app} [32]. The polarizability for a microsphere with relative permittivity ε_r in a medium with relative permittivity ε_m can be derived as [33]:

$$\alpha = 3\left(\frac{\varepsilon_r - \varepsilon_m}{\varepsilon_r + 2\varepsilon_m}\right)\varepsilon_0\varepsilon_m V \tag{5}$$

where V is the volume of the microsphere. This result can be extended to a dilute dispersion of microspheres with a volume fraction v within a host medium of relative permittivity ε_m, giving rise to an effective permittivity of the medium of

$$\varepsilon_{\mathrm{eff}} \approx \left[1 + 3V\left(\frac{\varepsilon_r - \varepsilon_m}{\varepsilon_r + 2\varepsilon_m}\right)\right]\varepsilon_m \tag{6}$$

3. Design Concepts

A. Sensor Design, and Simulation

The CGRR-based microwave microfluidic sensor presented in [30] offers high sensitivity resulting from its high Q compared to microwave microfluidic sensors reported in the literature, due to the surface current density redistribution; the surface current is distributed along the two opposite circumferential sides of the CGRR, thereby creating a high electric field in the capacitive gap between the two central posts. The surface losses are the due to the sum of $(H_s)^2$ over all resonator surfaces, with the surface magnetic field H_s proportional to the local current density. Making the current spread more uniformly across surfaces results in a lower surface loss, assuming the surface resistance remains constant.

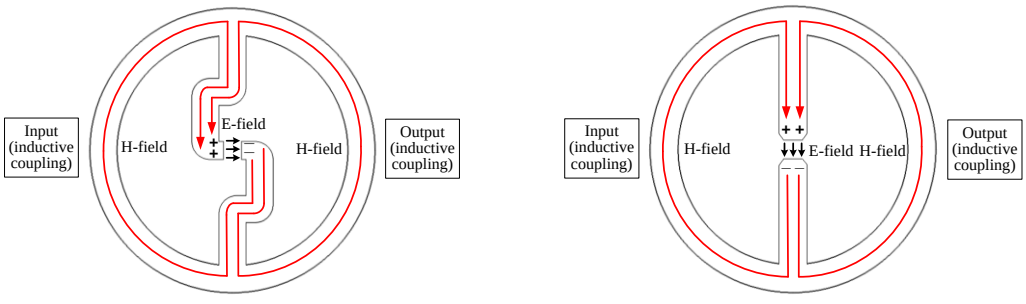

(a) (b)

Fig. 2. Schematic of charges, surface currents, and high electric field concentrated in the central gap space of (a) the first resonator, and (b) the second resonator. Both resonators are excited inductively using loop coupling.

Fig. 2 indicates the schematic distribution of the electric field and its direction for both resonators. The gap region serves as a sensing capacitor, where the electric field is concentrated. In contrast, the magnetic field is distributed on the circumference of the resonator, where the surface current is distributed for the high Q requirement. The inductive regions, where the H-field is concentrated, are formed by the circumferential sides. Here we locate the input and output ports using a symmetric pair of inductive coupling loops.

The geometric design parameters of both resonators are shown in Fig. 3. The outer radius of the ring is r_{out} = 15.5 mm, while the inner radius is r_{in} = 12.5 mm. The width of the central pillars is w=3mm, and a=2mm. The thickness of the ring is h=1 mm and the sensing gap length is d =2 mm. The sample tube is made from quartz, and has outer and inner diameters of 2 mm and 1.4 mm, respectively. The resonant frequency of the DCGRR sensor (when the sample tube is empty) is designed to be 2.36 GHz and 2.68 GHz for the first and second resonators, respectively. Designs were informed by iterative simulations using COMSOL Multiphysics 4.4, since even simple ring resonators have no exact design formulae. In both resonators the applied electric field is perpendicular to the sample tube in the sensing gap regions. The first resonator is fixed on an aluminum ground plate (of 1 mm thickness) using four cylindrical supports made from polytetrafluoroethylene (PTFE), a dielectric with very low loss, as shown in Fig. 4, which lift the resonator 2 mm from the ground plate. The second resonator was similarly fixed on same aluminum ground plate, as shown in Fig. 5. The outer cylindrical cavity has a depth and an inner diameter of 45 mm and 60 mm, respectively, chosen to attain a good separation between DCGRR resonant frequencies and resonances generated by the outer cavity itself. The purpose of the outer aluminum cavity is to reduce the radiation losses to ensure highest Q.

Small holes are drilled in the top and bottom lids of the outer cavity to insert the sample tube, and also two holes into sides of the cavity for the coupling feedlines. RG402 coaxial cable was used in the simulation to perform inductive coupling by extending its central conductor and bending it to form a half circle with a radius of 4 mm and then short circuited by connecting its end directly to the inner surface of the aluminum cavity, as in Fig. 4. The S-parameters of the two-port sensor are then measured using a vector network analyzer. The transmission coefficient S_{21} can be written [34]:

$$S_{21} = \frac{2\sqrt{g_1 g_2}}{g_1 + g_1 + 1 + 2jQ_0\left(\frac{f - f_0}{f_0}\right)} \tag{7}$$

where g_1, and g_2 are the coupling coefficients at port 1 and port 2, respectively, defined as:

$$g_1 = k_1 f_0 Q_0, \;\; g_2 = k_2 f_0 Q_0 \tag{8}$$

The values of constants k_1, and k_2 depend on the geometrical properties of the coupling loops (i.e. area of the loops and the distance between them and the resonator).

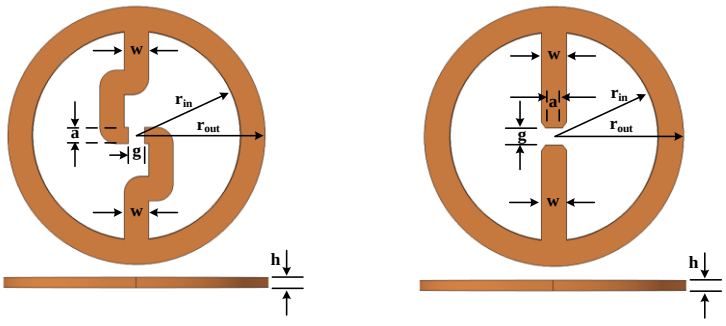

(a) (b)

Fig. 3. Dimension labels for (a) first, and (b) second resonators.

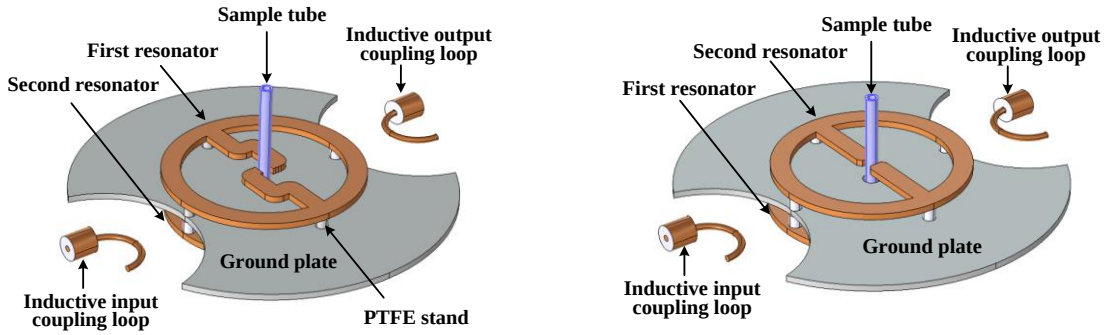

(a) (b)

Fig. 4. Designs of (a) the first resonator, and (b) the second resonator, both fixed on the same aluminum ground plate using four PTFE cylindrical posts for each resonator. The sample tube passes through the gaps of each resonator, where the electric field is highest.

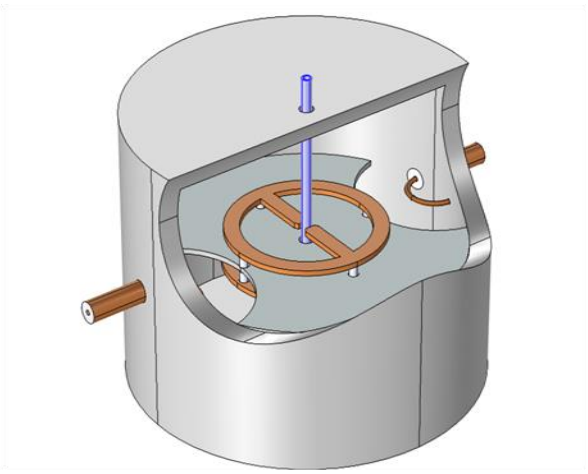

Fig. 5. The whole compact sensor consists of two resonators fixed on a central ground plate of the aluminum cavity, with a common axis.

The simulated electric field and voltage transmission coefficient $|S_{21}|$ are shown in Fig. 6 for both resonators. From $|S_{21}|$, the calculated quality factor Q is around 950 for each resonator. The electric field is localized in the gap region of each resonator, where the capillary passes, so there are two active regions with high electric field to test the same sample.

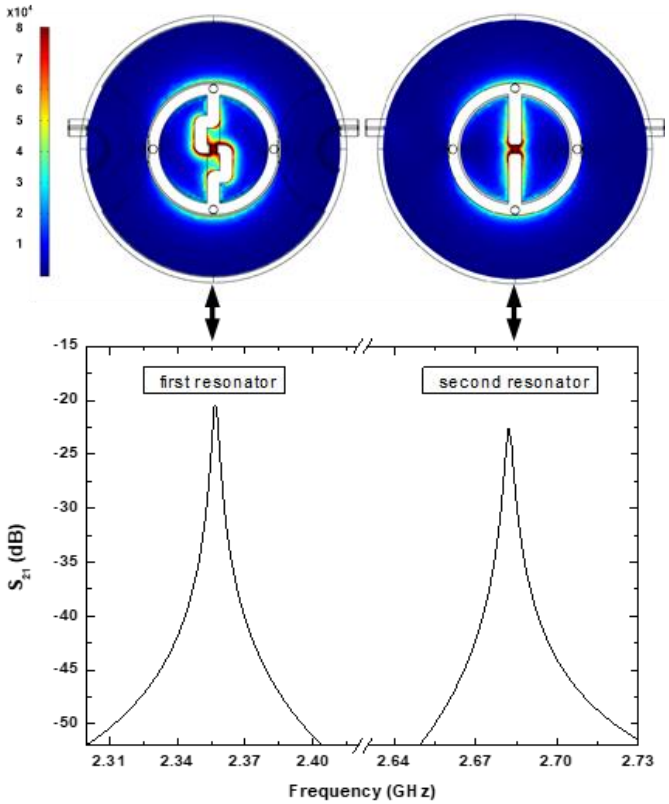

Fig. 6. Simulated electric field using COMSOL Multiphysics for each resonator, and the related $|S_{21}|$ traces.

B. Sensor Sensitivity

Sensitivity *S* is an important parameter for microwave microfluidic sensors, and for each resonator is calculated based on the simulation results shown in Table I. Several common solvents were used in these simulations using COMSOL Multiphysics, where the liquids' simulated permittivities are based on the Debye model and well-known Debye parameters [31].

Table I
Simulated Results for DCGRR's Resonant Frequency, Q-Factor, Insertion Loss, and Complex Permittivity when the Quartz Tube is Empty of Filled with Liquids

Resonator	Status	Simulated			Simulated Permittivity
		f_0 (GHz)	Q	IL (dB)	
First resonator	Empty	2.356	948	–20.43	
	Chloroform	2.322	469	–25.25	4.69 – j0.26
	Ethanol	2.306	68	–41.33	7.15 – j7.11
	Methanol	2.295	170	–34.34	22.6 – j13.0
	Water	2.287	610	–23.42	77.3 – j8.83
Second resonator	Empty	2.682	964	–22.56	
	Chloroform	2.645	405	–29.50	4.68 – j0.29
	Ethanol	2.629	72	–45.97	6.55 – j6.46
	Methanol	2.611	155	–39.50	20.9 – j13.3
	Water	2.602	624	–26.98	77.0 – j10.0

The sensitivity can be defined by [6]:

$$S = \frac{f_1 - f_0}{f_0(\varepsilon_1 - 1)} \times 100\% \quad (9)$$

[6]

where f_1, and f_0 is the resonant frequency of the resonator with and without the liquid, respectively.

The sensitivities of both resonators are closely matched, as shown in Fig. 7. It can be noted that sensitivity decreases with increasing real part of relative permittivity because the depolarization is then almost complete and further increases of ε_1 result in diminishingly smaller increases in the sample's dipole moment. In Fig. 8, the sensitivity of the proposed sensor versus ε_1 of the tested samples is compared with other microwave sensors based on the measured results in the literature. In [31], authors used a microstrip split-ring resonator operating at 3 GHz to measure the relative permittivity of some common liquids and in [35] a rectangular waveguide cavity tuned at 1.91 GHz. It can be seen that the sensitivity of the proposed sensor is higher than [35] when ε_1 is less than 23, and higher than [31] for the all tested values of ε_1. This is very helpful in dielectric characterization when the relative permittivity of the tested microplalets/particles is less than 23 (in our case the relative permittivity of microplatelet which is 2.1).

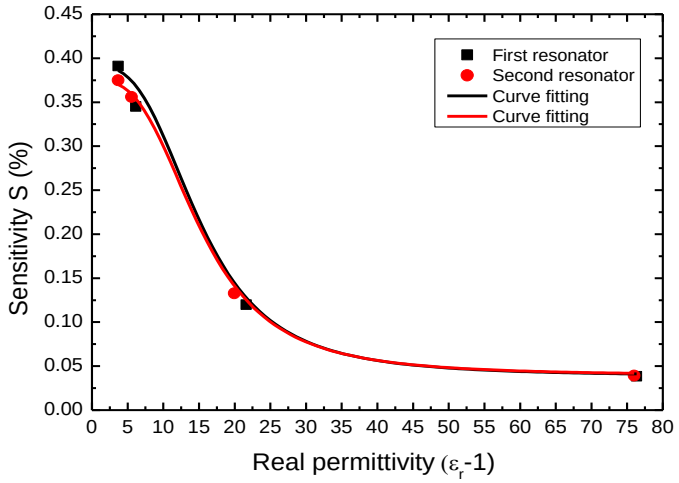

Fig. 7. Sensitivity of the DCGRR as a function of the sample's relative permittivity. Note that first and second resonator are approximately matched in sensitivity.

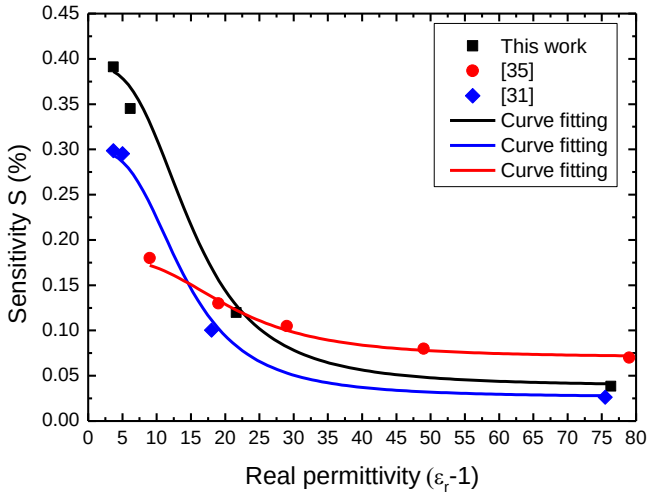

Fig. 8. Sensitivity comparison between the DCGRR reported here and other experimental sensors reported in the literature.

4. Sensor Fabrication

The sensor was manufactured as designed; the two resonators were made from copper, with the outer cavity turned from a solid aluminum cylinder. By this method a plate (of height 1 mm) is left in the middle of the cavity which as a central ground plate that separates the cavity's inner volume into two spaces, the upper space for the

first resonator and the lower space for the second resonator. These two resonators are fixed on that ground plate using four PTFE cylindrical stands for each resonator, as described previously in the sensor design. Two lids (top and bottom) are manufactured with a hole of 3 mm diameter for the capillary insertion. Furthermore, two holes were drilled in the cavity sides for the the RG402 coaxial feedline, terminated with SMA connectors. The final manufactured sensor is shown in Fig. 9.

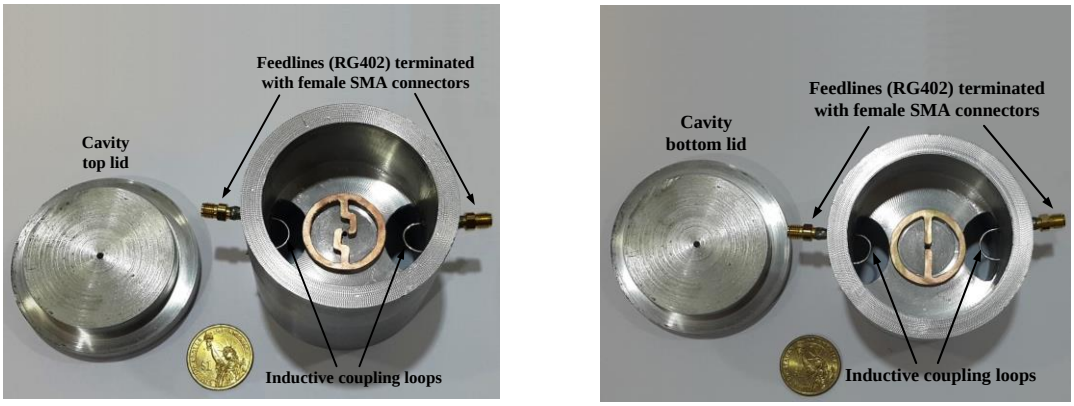

(a) (b)

Fig. 9. Manufactured sensor, (a) first resonator view from the top, (b) second resonator viewed from the bottom.

5. Results

A. Liquid Test Results

Initially the common solvents, water, methanol, ethanol and chloroform were tested using the DCGRR. The Debye model [28] was encoded into COMSOL to calculate the complex permittivity of the liquids for the simulations. The complex permittivity of liquids can be obtained from the measured resonant frequency and Q-factor extracted from S_{21}, using the following which are approximated from Eqs. (3) and (4):

$$\frac{f_1-f_0}{f_0} \approx -\mathrm{Re}\left(\frac{\varepsilon-1}{\varepsilon+1}\right)\frac{V_s}{V_m} \tag{10}$$

$$\frac{1}{Q_1}-\frac{1}{Q_0} \approx -2\,\mathrm{Im}\left(\frac{\varepsilon-1}{\varepsilon+1}\right)\frac{V_s}{V_m} \tag{11}$$

where V_s is the sample volume in the effective electric field and V_m is the mode volume resonator; this is the electrical energy stored in the cavity divided by the electrical energy density at the sample and can be calculated from the COMSOL simulations. The simulated and measured transmission coefficients $|S_{21}|$ are shown in Fig. 10, with data listed in Table II for the resonant frequency, quality factor and insertion loss of the DCGRR when the quartz tube is empty or filled with the solvents described above. There is excellent agreement between the measured and simulated data.

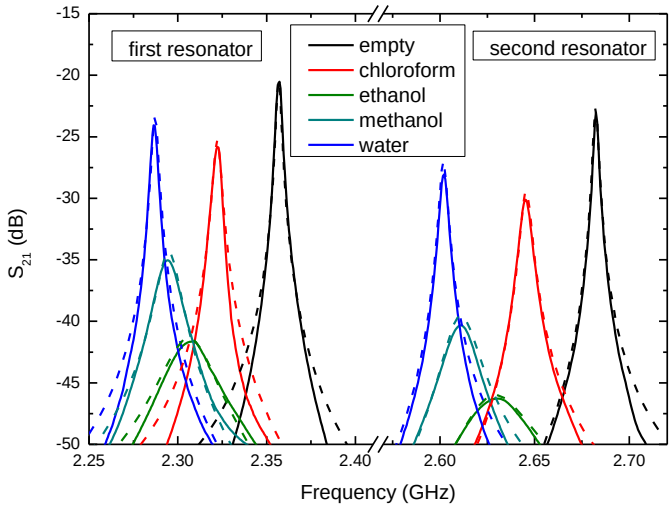

Fig. 10. Measured and simulated transmission coefficient $|S_{21}|$ for several common solvents at 25°C for the first and second resonators.

Table II
Simulated and Measured Results for DCGRR's Resonant Frequency, Q-Factor, Insertion Loss, and Complex Permittivity when the Quartz Tube is Empty of Filled with Liquids

Resonator	Status	Simulated				Measured			Simulated Permittivity	Measured Permittivity	Error %
		f_0 (GHz)	Q	IL (dB)		f_0 (GHz)	Q	IL (dB)			
First resonator	Empty	2.356	948	–20.43		2.357	943	–20.53			
	Chloroform	2.322	469	–25.25		2.322	465	–25.81	4.69 – j0.26	4.66 – j0.31	1.9
	Ethanol	2.306	68	–41.33		2.307	63	–41.64	7.15– j7.11	7.12 – j7.00	1.9
	Methanol	2.295	170	–34.34		2.294	166	–35.04	22.7 – j13.0	22.5 – j13.4	0.8
	Water	2.287	610	–23.42		2.286	602	–24.05	77.3 – j8.83	77. 1– j9.12	0.6
Second resonator	Empty	2.682	964	–22.56		2.682	958	–23.03			
	Chloroform	2.645	405	–29.50		2.645	400	–30.11	4.68 – j0.29	4.71 – j0.28	1.2
	Ethanol	2.629	72	–45.97		2.630	68	–46.28	6.55 – j6.46	6.61 – j6.51	1.7
	Methanol	2.611	155	–39.50		2.611	152	–40.33	20.9 – j13.3	21.2 – j13.1	0.8
	Water	2.602	624	–26.98		2.602	620	–28.05	77.0 – j10.0	77.2 – j9.95	0.6

b. Micro-Platelet Test Results

To test the sensor's ability to characterize the orientation of particles, measurements were performed on cylindrical, dielectric micro-platelets (diameter 1.2 mm, thickness 0.6 mm, relative permittivity 2.1) within a water medium, with the orientations shown in Fig. 11. The sensor will be sensitive for each micro-platelet when it is passes through the active region of both sensors, where the electric field is at maximum amplitude. The COMSOL simulated electric field in each orientation is shown in Fig. 12.

The dipole moment of the sample will be larger (i.e. larger internal field) when its edges are parallel to the gap faces of the second resonator ((b) in Fig. 11), compared with when its faces are parallel with the gap faces ((a) in Fig. 11). This is due to the depolarization of the electric field owing to the induced surface polarization charges, which is largest for the latter case; this is shown schematically in Fig. 13. The results for the micro-platelet in the two resonators are shown in Fig. 14, with excellent agreement between the simulated and measured results. This demonstrates the sensor's ability to discern the orientation of the micro-particles.

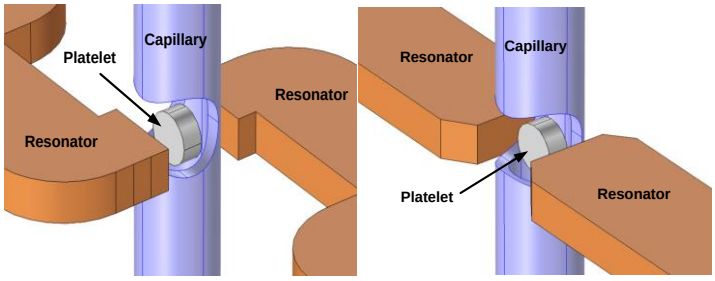

(a) (b)

Fig. 11. Microplatelet flowing in a water medium, (a) with its faces parallel to the gap faces of the first resonator, (b) with its side edges parallel to the gap faces of the second resonator.

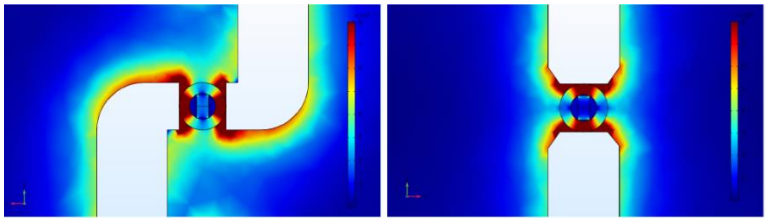

Fig. 12. Cross sectional top view of the COMSOL simulated electric field for the two resonators and micro-particle orientations shown in Fig. 11.

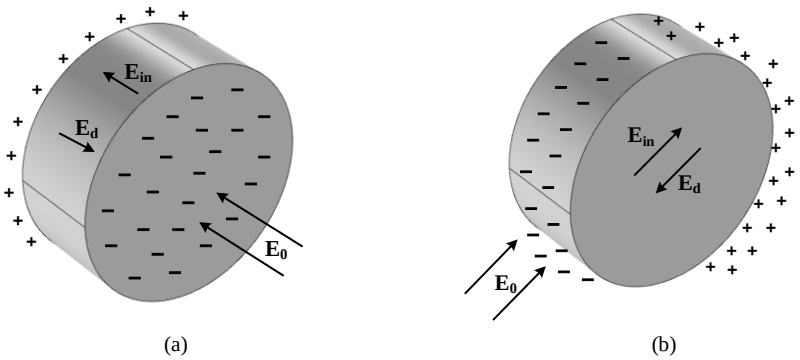

(a) (b)

Fig. 13. The depolarizing electric field E_d when the faces of the micro-platelet are perpendicular to the applied electric field E_0 (in (a)) is greater than when the edges of the micro-platelet are perpendicular to E_0 (in (b)).

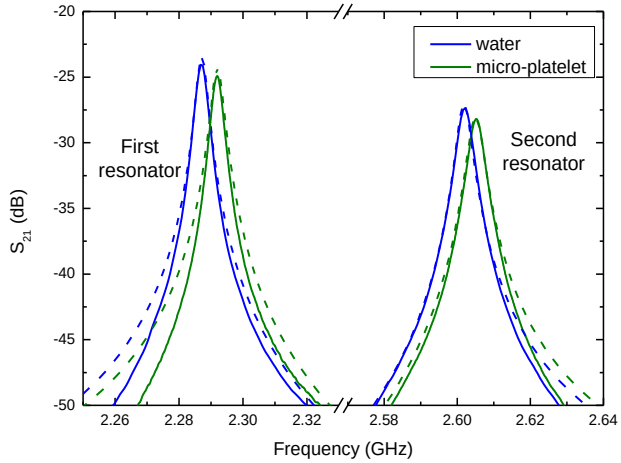

Fig. 14. Measured and simulated transmission coefficient $|S_{21}|$ when the micro-platelet passes though first and second resonators. The faces of the micro-platelet are parallel to gap faces of the first resonator (repeatability measurement error is 1 MHz), while its side edges are parallel to the gap faces of the second resonator (repeatability measurement error is 0.7 MHz), as in Fig. 11.

C. Emulsion Test Results

CALPOL® is a paracetamol suspension that is commonly used to lower a child's temperature and for pain relief. It consists of a aqueous suspension of solid micro-particles so is an ideal emulsion to test our sensor. We used it at a concentration of 250 mg/5ml to confirm the sensor's ability to assess a small change in concentration of a typical medical emulsion under the conditions of continuous flow. A syringe pump was used to inject the emulsion at a constant flow rate of 0.75 ml/min through the active gaps of both resonators. Initially, the resonant frequency of both resonators was recorded for 15 seconds time interval as the emulsion passes through the sensor, giving 2.314 GHz and 2.620 GHz for the first and second resonators, respectively. Then, the emulsion was diluted with 2%, 5%, 10%, and 15% of DI water (volume/volume) to get different emulsion concentrations of 98%, 95%, 90% and 85%, respectively. The resonant frequency was recorded at each concentration and the results are shown in Fig. 15. This demonstrates our sensor's high sensitivity to the emulsion concentration levels. Both resonant frequencies decrease with decreasing the emulation concentration with small amounts of water, as expected since the real part of the complex permittivity of water (around 80) is much greater than that of the solid phase (around 3). Similar effects as a function of concentration were observed for both resonators, as shown in Fig. 16. The maximum shift in the resonant frequency (Δf) is 18 MHz, which is larger than in [28, 29] leading to more accurate measurements.

We would not expect much difference in sensitivity for the two resonators in the measurement of emulsions since the micro-particles are approximate spheres and are randomly dispersed, with many thousands being sampled (and averaged) at any given time.

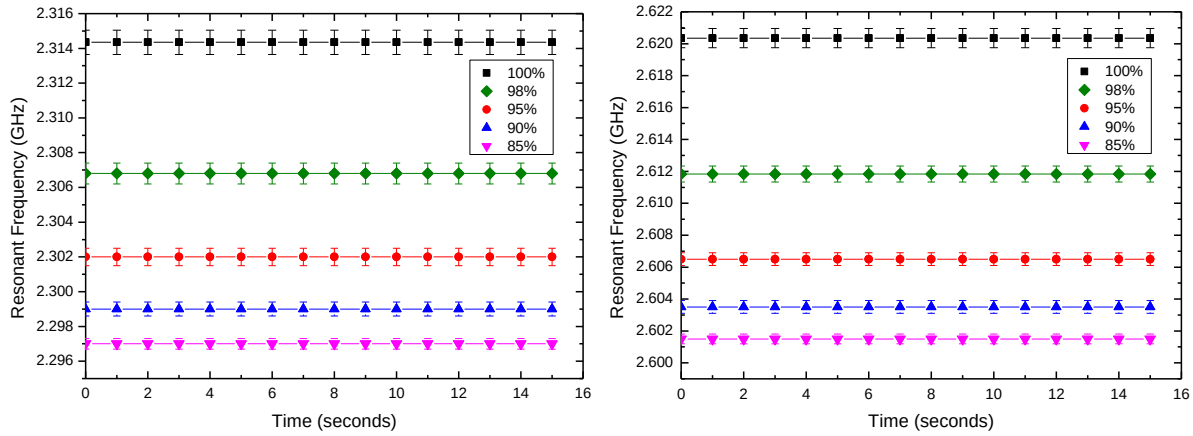

Fig. 15. Measured resonant frequency for different concentrations of CALPOL® at a flow rate of 0.75 ml/min, (a) first resonator, (b) second resonator. Both resonant frequencies decrease with lower concentrations.

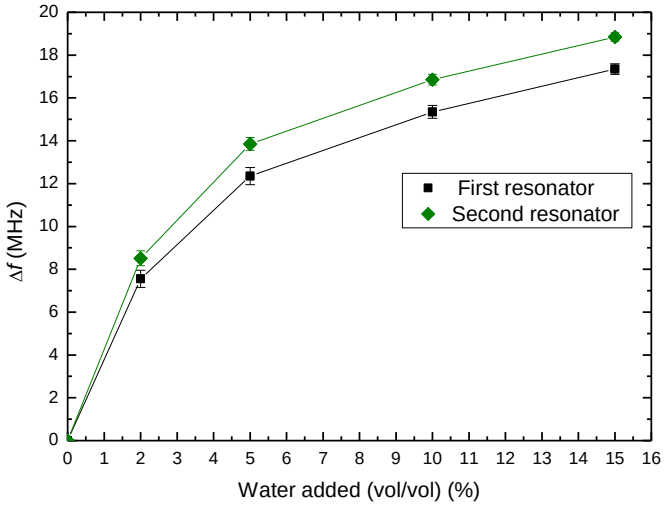

Fig. 16. Measured change in resonant frequency for different concentrations of CALPOL® for the two resonators, exhibiting common behaviour.

6. Conclusions

A compact microwave sensor using dual resonators has been proposed for micro-platelet and emulsion detection and characterization. The sensing operation is based on the microwave resonator perturbation theory. COMSOL Multiphysics was used in the sensor design and optimization, and there was very good agreement between simulation and experimental results. The micro-platelets detection occurs when they are within a water medium and flow in a microfluidic channel, which passes through the active (i.e. capacitive) gap regions of both resonators, where the microwave electric field is at its maximum value. These gaps represent the sensing zones which induce polarization in the samples, with two orthogonal directions of the applied microwave electric field to extract more information, especially regarding microplatelet orientation. The sensor has also been applied successfully to assess emulsion concentrations under flow conditions for pharmaceutical applications. CALPOL® which is a paracetamol suspension has been utilized for this purpose. This sensor is compact, highly sensitive, easy to interface with associated microfluidic components, and cheap to manufacture and also to interrogate with a scalar microwave instruments, e.g. as the tank circuit for an oscillator, given that emulsion concentrations is readily assessed from changes in resonant frequency alone.

References

[1] M. Peichl, T. Albers, and S. Dill, "Detection of small impurities in bulk material by MMW radar." pp. 294-299.

[2] L. Su, X. Huang, W. Guo, and H. Wu, "A flexible microwave sensor based on complementary spiral resonator for material dielectric characterization," *IEEE Sensors J.*, 2019.

[3] A. Foudazi, and K. M. Donnell, "Effect of sample preparation on microwave material characterization by loaded waveguide technique," *IEEE Trans. Instrum. Meas.,* vol. 65, no. 7, pp. 1669-1677, 2016.

[4] R. E. Ghiri, and K. Entesari, "A miniaturized UWB microwave dual-comb dielectric spectroscopy system," *IEEE Trans. Microw. Theory Techn.,* vol. 67, no. 12, pp. 5218-5227, 2019.

[5] A. A. Abduljabar, H. Hamzah, and A. Porch, "Multi-resonators, microwave microfluidic sensor for liquid characterization," *Microwave and Optical Technology Letters,* 2020.

[6] A. Ebrahimi, J. Scott, and K. Ghorbani, "Ultrahigh-sensitivity microwave sensor for microfluidic complex permittivity measurement," *IEEE Trans. Microw. Theory Techn.,* vol. 67, no. 10, pp. 4269-4277, 2019.

[7] B. D. Wiltshire, T. Zarifi, and M. H. Zarifi, "Passive split ring resonator tag configuration for RFID-based wireless permittivity sensing," *IEEE Sensors J.,* 2019.

[8] P. Vélez, L. Su, K. Grenier, J. Mata-Contreras, D. Dubuc, and F. Martín, "Microwave microfluidic sensor based on a microstrip splitter/combiner configuration and split ring resonators (SRRs) for dielectric characterization of liquids," *IEEE Sensors J.,* vol. 17, no. 20, pp. 6589-6598, 2017.

[9] J. Dong, F. Shen, Y. Dong, Y. Wang, W. Fu, H. Li, D. Ye, B. Zhang, J. Huangfu, and S. Qiao, "Noncontact measurement of complex permittivity of electrically small samples at microwave frequencies," *IEEE Trans. Microw. Theory Techn.,* vol. 64, no. 9, pp. 2883-2893, 2016.

[10] C.-K. Lee, S. Zhang, S. S. Bukhari, D. Cadman, J. Vardaxoglou, and W. G. Whittow, "Complex permittivity measurement system for solid materials using complementary frequency selective surfaces," *IEEE Access,* vol. 8, pp. 7628-7640, 2020.

[11] H. Choi, J. Naylon, S. Luzio, J. Beutler, J. Birchall, C. Martin, and A. Porch, "Design and in vitro interference test of microwave noninvasive blood glucose monitoring sensor," *IEEE Trans. Microw. Theory Techn.,* vol. 63, no. 10, pp. 3016-3025, 2015.

[12] K. K. Adhikari, and N.-Y. Kim, "Ultrahigh-sensitivity mediator-free biosensor based on a microfabricated microwave resonator for the detection of micromolar glucose concentrations," *IEEE Trans. Microw. Theory Techn.,* vol. 64, no. 1, pp. 319-327, 2015.

[13] K. Grenier, D. Dubuc, P.-E. Poleni, M. Kumemura, H. Toshiyoshi, T. Fujii, and H. Fujita, "Integrated broadband microwave and microfluidic sensor dedicated to bioengineering," *IEEE Trans. Microw. Theory Techn.,* vol. 57, no. 12, pp. 3246-3253, 2009.

[14] H.-W. Wu, "Label-free and antibody-free wideband microwave biosensor for identifying the cancer cells," *IEEE Trans. Microw. Theory Techn.,* vol. 64, no. 3, pp. 982-990, 2016.

[15] H. Hamzah, E. Ahortor, D. Malyshev, H. Choi, J. Lees, L. Baillie, and A. Porch, "A compact microwave applicator for the rapid detection of clostridium difficile." pp. 1-4.

[16] R. A. Alahnomi, Z. Zakaria, E. Ruslan, S. R. Ab Rashid, and A. A. M. Bahar, "High-Q sensor based on symmetrical split ring resonator with spurlines for solids material detection," *IEEE Sensors J.,* vol. 17, no. 9, pp. 2766-2775, 2017.

[17] F. Artis, D. Dubuc, J.-J. Fournié, M. Poupot, and K. Grenier, "Microwave dielectric spectroscopy of cell membrane permeabilization with saponin on human B lymphoma cells." pp. 1-4.

[18] T. Chen, D. Dubuc, M. Poupot, J.-J. Fournie, and K. Grenier, "Accurate nanoliter liquid characterization up to 40 GHz for biomedical applications: Toward noninvasive living cells monitoring," *IEEE Trans. Microw. Theory Techn.,* vol. 60, no. 12, pp. 4171-4177, 2012.

[19] P. Mehrotra, B. Chatterjee, and S. Sen, "EM-wave biosensors: A review of RF, microwave, mm-wave and optical sensing," *Sensors,* vol. 19, no. 5, pp. 1013, 2019.

[20] A. Tamra, D. Dubuc, M.-P. Rols, and K. Grenier, "Microwave monitoring of single cell monocytes subjected to electroporation," *IEEE Trans. Microw. Theory Techn.,* vol. 65, no. 9, pp. 3512-3518, 2017.

[21] W. Chen, D. Dubuc, and K. Grenier, "Microwave dielectric spectroscopy of a single biological cell with improved sensitivity up to 40 GHz." pp. 1-3.

[22] T. Chen, F. Artis, D. Dubuc, J. Fournie, M. Poupot, and K. Grenier, "Microwave biosensor dedicated to the dielectric spectroscopy of a single alive biological cell in its culture medium." pp. 1-4.

[23] F. Deshours, G. Alquié, H. Kokabi, K. Rachedi, M. Tlili, S. Hardinata, and F. Koskas, "Improved microwave biosensor for non-invasive dielectric characterization of biological tissues," *Microelectronics Journal,* vol. 88, pp. 137-144, 2019.

[24] D. Dubuc, O. Mazouffre, C. Llorens, T. Taris, M. Poupot, J.-J. Fournié, J.-B. Begueret, and K. Grenier, "Microwave-based biosensor for on-chip biological cell analysis," *Analog Integr. Circuits Signal Process,* vol. 77, no. 2, pp. 135-142, 2013.

[25] M. Nikolic-Jaric, S. Romanuik, G. Ferrier, G. Bridges, M. Butler, K. Sunley, D. Thomson, and M. Freeman, "Microwave frequency sensor for detection of biological cells in microfluidic channels," *Biomicrofluidics,* vol. 3, no. 3, pp. 034103, 2009.

[26] C.-F. Liu, M.-H. Wang, and L.-S. Jang, "Microfluidics-based hairpin resonator biosensor for biological cell detection," *Sens. Actuators B: Chem.,* vol. 263, pp. 129-136, 2018.

[27] S. Mohammadi, R. Narang, M. Mohammadi Ashani, H. Sadabadi, A. Sanati-Nezhad, and M. H. Zarifi, "Real-time monitoring of Escherichia coli concentration with planar microwave resonator sensor," *Microw. and Opt. Techn. Lett.,* vol. 61, no. 11, pp. 2534-2539, 2019.

[28] M. Abdolrazzaghi, M. H. Zarifi, C. F. Floquet, and M. Daneshmand, "Contactless asphaltene detection using an active planar microwave resonator sensor," *Energy & Fuels,* vol. 31, no. 8, pp. 8784-8791, 2017.

[29] M. Abdolrazzaghi, M. H. Zarifi, M. Daneshmand, and C. F. Floquet, "Contactless asphaltene solid particle deposition monitoring using active microwave resonators." pp. 1-3.

[30] H. Hamzah, A. A. Abduljabar, and A. Porch, "High Q microwave microfluidic sensor using a central gap ring resonator," *IEEE Trans. Microw. Theory Techn.,* vol. 68, no. 5, 2020.

[31] A. A. Abduljabar, D. J. Rowe, A. Porch, and D. A. Barrow, "Novel microwave microfluidic sensor using a microstrip split-ring resonator," *IEEE Trans. Microw. Theory Techn.,* vol. 62, no. 3, pp. 679 - 688 Mar., 2014.

[32] D. J. Griffiths, and R. College, *Introduction to electrodynamics,* 3rd ed., New Jersey, USA: Prentice Hall, 1999.

[33] A. Sihvola, "Dielectric Polarization and Particle Shape Effects," *Journal of Nanomaterials,* vol. 2007, pp. 1-9, 2007.

[34] M. J. Lancaster, *Passive microwave device applications of high-temperature superconductors*: New York : Cambridge University Press, 1997.

[35] G. Gennarelli, S. Romeo, M. R. Scarfì, and F. Soldovieri, "A microwave resonant sensor for concentration measurements of liquid solutions," *IEEE Sensors J.,* vol. 13, no. 5, pp. 1857-1864, 2013.

Ali A. Abduljabar received the B.Sc. and M.Sc. degrees in electrical engineering from the University of Basrah, Basrah, Iraq, and the Ph.D. degree in electrical engineering from Cardiff University, Cardiff, U.K.
He is currently a Lecturer in microwave engineering with the University of Basrah. His current research interests include the design of microwave sensors for microfluidic systems and noninvasive applications and microwave heating techniques.

Hayder Hamzah received the B.Sc. and M.Sc. degrees in electronic and communications engineering at Nahrain University, Baghdad, Iraq, and Ph.D. degrees in microwave engineering from Cardiff University, Wales, UK. He is currently a senior lecturer at Engineering College/University of Al-Qadisiyah. His research activities include design of microwave sensors and applicators for microfluidic systems.

Adrian Porch received the M.A. degree in physics and Ph.D. degree in low-temperature physics from Cambridge University, Cambridge, U.K. He is a Professor with the School of Engineering, Cardiff University, Cardiff, U.K., and leads the Centre for High Frequency Engineering. He has over 30 years of experience in applying microwave methods to measure and understand the fundamental properties of electronic materials. More recently, his techniques have been used to develop new types of electromagnetic sensors, with emphasis on applications across different disciplines.